Novel Ғ-Slotted Wideband Antenna for Sub-6 GHz 5G Applications and Gain Enhancement using Freuency-Selective Surface

Chandra Shekhar Rajora[1], Prem Pal Singh[2*], Sudhir Kumar Sharma[3]

[1,3]Department of ECE, Jaipur National University, Jaipur, India

[2]Department of ECE, Parul Institute of Engineering and Technology, Parul University, Vadodara, Gujarat, India

[*]Corresponding Author: Prem Pal Singh, Mob.- +91-8426090558
[1]chandra.shekhar@jnujaipur.ac.in, [2]prempal.singh38023@paruluniversity.ac.in, [3]sudhir.732000@gmail.com
Postal Address: Department of ECE, Parul Institute of Engineering and Technology, Parul University, Vadodara, Gujarat-391760, India

Abstract: This paper presents an antenna operating from 3.44 to 6.45 GHz, integrated with a frequency-selective surface (FSS) to enhance gain. The physical size of the antenna is 22 × 29 × 0.8 mm³, and the electrical size is 0.249λ × 0.329λ × 0.009λ at 3.4GHz. The antenna geometry consists of a modified elliptical patch with a 'F' slot and a stepped slotted partial ground plane, which helps achieve a wideband response. The maximum gain of the antenna is 4 dBi. Furthermore, to enhance the antenna's gain and improve the bandwidth, a modified cross-shaped frequency-selective surface structure with a 4×4 array is designed and fabricated. The total dimensions of the unit cell and 4×4 array are 18 mm × 18 mm and 80 mm × 80 mm, respectively. This FSS is positioned at an optimized distance of H = 22.2 mm from the antenna to achieve high gain and maintain a wideband response. Using FSS, an improvement in gain is observed, with a maximum of 8.62 dBi. Additionally, an improvement in the bandwidth is observed. The FSS extended the bandwidth from 3.18 GHz to 6.40 GHz. The prototype of the suggested antenna and FSS has been fabricated and tested, and the results indicate that the simulated and measured values match closely, except for minor deviations due to fabrication and testing tolerances.

Keywords: Wideband Antenna, 5G, Sub-6 GHz, Frequency Selective Surface, High gain, FR-4

Accepted by Scientia Iranica

1. Introduction

Wireless devices are increasing in number daily with advancements in communication systems. Over the last 2-3 years, the primary focus has been on improving performance and minimizing the size of communication system [1], and the antenna plays a vital role in any communication system as it is a crucial component of any communication system to maintain performance stability [2], [3]. A wideband antenna with high gain is essential for many applications, including 5G. Antennas with high gain and improved bandwidth can enhance the performance of the current communication system. These performance parameters include gain, bandwidth, efficiency, radiation pattern and directivity. Over the past few years, wireless and space communication have seen significant advances and require high data rates. Hence, to achieve this, high-gain, wideband antennas are key elements [4]. A wideband response can be achieved by creating defected ground structures. 5G technology is now providing faster and more secure networks, along with low latency. The sub-6 GHz band is assigned to 5G services by the Federal Communications Commission (FCC). Different frequencies are used for 5G applications across various sub-6 GHz bands in multiple countries worldwide, as summarized in Table 1 [5]. This band enables high-speed wireless communication over long distances, and achieving these performance levels requires a high-performance antenna [6]. Due to advancements in wireless technology, wideband antennas are required to operate on multiple bands simultaneously [7]. Wideband antennas cover a broad frequency spectrum, making them particularly useful for 5G applications. There are several issues with sub-6 GHz antennas, including low gain and efficiency, as well as a narrow bandwidth. Various techniques are available to improve the mentioned parameters, and the use of a Frequency Selective Surface (FSS) is one of them, which helps reduce back radiation, boosting gain and improving bandwidth.

In recent years, numerous antenna designs have been developed to enhance the performance of existing antennas. In [8], a circular-loop-shaped FSS-based antenna was presented for 5G applications over the frequency range of 3.6-6.1 GHz. The antenna is designed on a FR-4 substrate with a thickness of 1.6 mm. Without FSS, the antenna size is 30 mm × 30 mm, and the unit cell size is 14 mm × 14 mm. The FSS used is a 7×7 array. The FSS is positioned 28.6 mm below the antenna. A gain enhancement of about 4 dB is obtained. A similar semi-circular slotted antenna loaded with FSS for 5G sub-6 applications was designed in [9]. The antenna operates in the n77 and n78 bands. The unit cell of FSS is a hexagonal-shaped structure, arranged as a 6×3 array to enhance gain and directivity.

In [10], a dual-band FSS was proposed to enhance the gain of an ultra-wideband antenna (UWB). The developed U-shaped antenna exhibited a wideband response from 3.15 to 22.65 GHz. FSS also helps improve the isolation and gain of MIMO antennas. Such type of antenna was developed in [11] with a ring-shaped FSS operating from 23.57 to 39.35 GHz. A gain improvement of more than 5 dBi was achieved. Single-layer FSS structures are easy to develop and can provide consistent gain with a wide range [12]. A wearable bow-tie-type antenna integrated with an FSS structure for wearable applications was designed to operate over a wide frequency range from 4.7 to 9 GHz [13]. A gain enhancement of 6.7 dBi was observed at a lower frequency of around 5 GHz. The antenna occupies an area of 27.5 mm × 27 mm. The

Accepted by Scientia Iranica

FSS array measures 45 mm × 45 mm and is placed 12.5 mm away to achieve the desired level of gain.

Similar antennas are used for UWB applications [13], [14], [15], dual-band applications [16], [17], [18] and on-body applications [19]. Antennas of various shapes for a wideband response can be designed using monopole or fractal geometries [20]. Defected ground structure (DGS) is another method for obtaining a wideband antenna, in which defects or slots are created in the ground plane [21]. The primary purpose of using FSS is to enhance gain, directivity, and bandwidth, and to minimise mutual coupling in MIMO antennas. Single-antenna systems without FSS provide low gain, which is undesirable for specific applications. In [22], the antenna without FSS operates on multiple bands; however, its gain is insufficient except at higher frequencies. A MIMO antenna with a wideband response from 3.33 to 5.04 GHz was designed in [23] to enhance gain and isolation. FSS also helps in minimizing SAR levels in wearable antennas [24]. This way, FSS integrated with the antenna improves the antenna's performance parameters. Methods discussed in the literature to enhance antenna gain include Artificial Magnetic Conductors (AMCs), Electromagnetic Bandgap Structures (EBGs), and FSSs. Primary limitations of these methods in the previous literature include narrow response, low efficiency, complex structures, and large size.

From the above analysis, it was found that, unlike the antennas in the published papers, the proposed antenna has a higher gain of 8.62 dBi. Also, the antenna with FSS in this paper provides a higher gain than the other antennas. Similarly, the designs in published works were complex and large, whereas the proposed antenna is compact, measuring 22 mm × 29 mm. Also, the antennas have a narrow bandwidth (BW < 2 GHz), compared to the proposed antenna (BW > 3 GHz). So, the contribution in this work includes (i) the integration of FSS with a small area compared to other reported antennas with an improvement in gain, (ii) a single-element antenna is smaller in size with no complex structure, (iii) offers a wide bandwidth in the sub-6 GHz band, which is essential for 5G applications in this band.

The FSS-backed antennas enhance the gain, but there are challenges, too. Integration of an FSS with the antenna is sensitive to changes in the reflection phase, the gap between antenna and FSS, and fabrication tolerances, as slight deviations can affect the antenna's gain and other performance parameters. Also, with a large gap between the antenna and the FSS, the space occupied is large. Other conventional methods for gain improvement have been discussed in the literature, such as the Electromagnetic Band Gap Structure (EBGs), dielectric superstrates [25] and an array antenna [26], [27]. These methods enhance antenna performance, but for wideband antennas, they are rarely suitable. Another challenge with the proposed antenna is the use of a FR-4 substrate, as dielectric losses may increase at high frequencies. To reduce losses, other materials such as Rogers RO4003 and RO3003, with low dielectric loss tangents, could be used.

So, this proposed work presents a wideband antenna operating from 3.44 to 6.45 GHz, with a bandwidth of 3.1 GHz. It has a compact size of 22 × 29 mm². Additionally, an FSS is integrated with the antenna, enhancing its gain. Along with the simulation and fabrication prototype, both the antenna and the FSS are represented as equivalent circuit models (ECM). The developed antenna is novel in terms of several features, as given below:

Accepted by Scientia Iranica

- The antenna is compact with a size of 22 × 29 mm², which operates initially from 3.5 GHz to 6.5 GHz.
- To enhance the bandwidth and gain, an FSS is integrated, then the operating band is extended to 3.18 GHz–6.40 GHz, achieving bandwidth enhancement and gain improvement.
- The gain of the antenna is improved from 4 dBi to 8.62 dBi using the FSS placed beneath the antenna without increasing the antenna size.
- The proposed antenna is suitable for 5G sub-6 GHz and C-band wireless communication systems.
- There is no active component used for gain enhancement, which maintains a simple and energy-efficient design.

The paper is structured as follows: Section 2 explains the geometric layout, the antenna's evolution, and the parametric analysis. Section 3 describes the design geometry and S-parameters of the suggested frequency-selective surface. The antenna results and their comparison with those obtained using FSS are presented in Section 4. Section 5 presents a comparison of the proposed antenna with those developed in the literature. Finally, the paper is concluded in Section 6.

2. Antenna Design Geometry

This section of the paper discusses the antenna geometry, the electronic equivalent circuit, and the stages of evolution. The reflection coefficients for the different evolutionary stages are also presented in this section. The antenna simulation is performed using the high-frequency structure simulator (HFSS), and the results are verified by developing a hardware prototype of the proposed antenna.

2.1. Antenna Design Geometry and Evolution

A. Geometry of Antenna

The geometric layout of the proposed antenna is shown in Figure 1. The physical size of the antenna is 22 mm × 29 mm. The antenna is simulated using the FR-4 substrate having a thickness of 0.8 mm and a dielectric constant of 4.4. The top side of the antenna is an elliptical-shaped patch with a F-shaped slot. Antenna performance in terms of bandwidth, radiation pattern, and gain is improved using a defected ground structure (DGS), in which defects are etched into the ground plane to alter the current distribution. This modification creates multiple resonances, resulting in a broad bandwidth [28], [29]. So, at the bottom side of the substrate, a staircase-slotted ground plane measuring 22 mm × 7.4 mm is placed. The F-shaped slot is introduced in the antenna patch to improve impedance matching and slightly enhance the bandwidth. The antenna layout is illustrated in Figure 1, and the antenna's design parameters are summarised in Table 2.

The proposed antenna is represented by an equivalent circuit, as shown in Figure 2(a). Wideband antenna behavior can be achieved by combining adjacent resonances. This circuit is simulated in Advanced Design System (ADS) as two parallel RLC circuits to achieve a wideband response through multiple resonances, and a series LC circuit to further broaden the bandwidth [30].

The primary resonance frequency of the circuit is calculated using basic series-parallel circuit

Accepted by Scientia Iranica

calculations, as described in [30]. The reflection coefficients obtained by simulation using HFSS and Circuit in ADS are compared in Figure 2(b), and the component values are summarized in Table 3, which were calculated using equations (1) and (2) [31] and the process followed in [30].

$$C = \frac{Q_T}{2\pi R f_r} \quad (1)$$

$$L = \frac{R}{2\pi f_r Q_T} \quad (2)$$

In equations (1) and (2),

$$R = \frac{h^2 E_0^2 j_n^2 \left(k_\rho\right)}{2P_T}$$

$j_n k_\rho$ is the Bessel function of order 'n', and Q_T is the total quality factor of the resonator, P_T is the power loss in the cavity, and fr is the resonant frequency of the antenna.

B. Design Evolution

This section discusses the design steps of the proposed antenna. Five design steps are involved in obtaining the final antenna. Figure 3 illustrates all five design steps, while Figure 4 shows the S-parameters of each design step.

The antenna design process began with selecting a target resonant frequency of 4 GHz. Based on this requirement, the initial major and minor radii of the elliptical patch were chosen as 9.8 mm and 10.48 mm, respectively. The area of the ellipse is given by [32]

$$A = \pi r^2 = \pi a.b \quad (3)$$

In equation (3), a and b are the major and minor radii, respectively

From equation (3)

$$r = \sqrt{a.b} \quad (4)$$

$$r = 10.13 \text{ mm}$$

The resonant frequency of a circular or elliptical patch for the first dominant mode (TM_{11}) is given by

$$f = \frac{1.8412 \times v_o}{2\pi a_{eff} \sqrt{\varepsilon_r}} \quad (5)$$

a_{eff} is the effective radius of the patch, which can be found using equation (6) [33].

$$a_{eff} = r.\left[1 + \frac{2h}{\pi r \varepsilon_r}\left(ln\left(\frac{\pi r}{2h}\right) + 1.7726\right)\right]^{1/2} \quad (6)$$

Accepted by Scientia Iranica

$$a_{eff} = 10.13\sqrt{1+\frac{2\times 0.8}{\pi\times 10.13\times 4.4}\left(ln\left(\frac{\pi\times 10.13}{2\times 0.8}\right)+1.7726\right)}$$

a_{eff} is the fringing field corrected radius

a_{eff} = 10.401 mm

The expected resonant frequency with an effective radius of 10.401 mm using equation (5) is given as

$$f_r = \frac{1.8412\times 3\times 10^8}{2\pi\times 10.401\times 10^{-3}\sqrt{4.4}} = 3.81GHz$$

The estimated full-ground resonant frequency was approximately 3.81 GHz. However, the simulated response of this initial configuration produced a resonance near 3.93 GHz with poor impedance matching ($S_{11} \approx -4.5$ dB), indicating poor coupling and a mismatch between the analytical model and practical current distribution. To improve this, the ground plane length was reduced from 29 to 7.4 mm in the second step.

With this modification, the antenna became a monopole-like radiator, thereby enhancing the fringing fields. As a result, it shifted the resonant frequency upward, improving the impedance bandwidth. In the next step, the partial ground plane was modified with a multi-stepped structure in the upper middle-centre of the ground, resulting in the shape known as step-3. This modification improved bandwidth and provided a wideband response, but again, impedance matching was poor. The antenna in this step of the design evolution did not yield the required results, as shown in Figure 4. In step 4, a F-shaped slot was etched into the radiating patch. With these modifications, the antenna's impedance matching has been improved.

Finally, to further enhance the matching, the patch is modified with two rectangular slots on the right and left sides. Some parameters were also optimized in this step to achieve the desired bandwidth and return loss. The return loss parameters of all four design steps are shown in Figure 4. The size of the substrate was selected as follows:

Length (L_{Sub}) = L_f+2r+3h (7)

L_{Sub} = 7+2×10.13+3×0.8=29.66 mm

Width (W_{Sub}) = 2×r-2t+6h (8)

W_{Sub} = 2×10.13-2×1.2+6×0.8

20.26-2.4× 4.8 =22.66 mm

Accepted by Scientia Iranica

Using equations (7) and (8), the calculated length and width of the substrate were 29.66 mm and 22.66 mm, respectively. So, the final length and width of the substrate were selected as 29 and 22 mm, respectively.

C. Parametric Analysis

The purpose of parametric analysis is to confirm the structure of the suggested antenna. In this parametric analysis, four dimensions (W_1, W_2, W_4, L_g) have been considered, as these dimensions directly influence the antenna's characteristics (S-parameters). To perform the parametric analysis, one parameter was varied while the other three were kept unchanged. The variation in S-parameters with different dimensions is shown in Figure 5. In Figure 5(a), W_1 was varied to investigate its effect on the resonance frequency and impedance matching.

Increasing W_1 beyond its optimal value shifts the frequency downward. Decreasing the W_1 affects the impedance matching. When W_2 is increased or decreased, impedance matching of the second resonance is affected. Also, the resonance frequency shifts to the lower side. This effect of W2 variation is shown in Figure 5(b). Impedance matching is also concerned with the variation in W_4; lower resonances shift to the right. However, the S11 increases at lower resonances but decreases at higher resonances, as illustrated in Figure 5(c).

Finally, the impact of the ground length, L_g, was analyzed. When L_g increases, the upper resonance frequency shifts to the left. The bandwidth of the antenna also decreases. When L_g decreases, the S_{11} of the antenna decreases across the complete band of operation. The optimized value of L_g is 7.4 mm, at which the antenna operates very well over a wide bandwidth. This impact on S_{11} and bandwidth is shown in Figure 5(d). These four parameters were selected due to their significant impact on S-parameters and bandwidth. The effect of the variation in these parameters on S_{11}, resonance frequency, and bandwidth is shown in Figure 5

D. Surface Current Distribution

Figure 6(a)-6(c) illustrates the surface current distribution at three different frequencies, 4, 5, and 6 GHz. Surface current analysis is necessary to understand the antenna's operation, as current density varies with operating frequency. At 4 GHz, the surface current is concentrated along the feed line and on a small portion of the lower patch edge. Additionally, the surface current is focused on the ground plane beneath the feed line and stepped structure. Similarly, at 5 GHz, the surface current is concentrated at the feed line as well as at the edges of the patch around the F-shaped slot. In the ground plane, the surface current pattern is similar to that at 4 GHz. At 6 GHz, the current is maximum at the left and right edges of the patch and the edges of the horizontal part of the F-shaped slot.

Accepted by Scientia Iranica

The current is also distributed at the feed line. As the frequency changes, the path of the surface current changes. Different portions and paths are responsible for generating new frequencies. The F-shaped slot enhanced the antenna's bandwidth. In the absence of this slot, the antenna does not radiate efficiently, and it also affects the S-parameters. As shown in Figures 6(b) and (c), this slot modifies the surface current by creating multiple current paths. This effect generates different closely spaced resonant modes. It is clearly observed from figures 6(a), (b), and (c) that the current concentration is strong along the edges of the F-slot. This indicates that this slot is responsible for the wideband response and actively participates in the radiation. In the absence of this slot, the antenna radiates weakly with non-uniform current distribution. This results in poor impedance matching. When this slot is removed from the patch, the surface current distribution is poor, leading to poor radiation and impedance matching. To show the effect of the slot, an additional surface current has been included for comparison at 4, 5, and 6 GHz, as shown in Figure 6(d). The S-parameters of the antenna without the F-slot are shown in Figure 6(e).

As evident from figures 6(a), (b) and (c), the F-slot modifies the surface current distribution as etching of this slot in the patch, introducing additional inductive and capacitive loading in the patch. As a result of this change, impedance matching improved at the upper frequency, 5.67 GHz. This behavior is clearly evident in the impedance plot. Figure 6 (f) shows the impedance of the antenna with and without F-shaped slot. Without this slot, the real part of the impedance at the upper resonant frequency of 5.67 GHz deviates from 50 Ω, while the imaginary part exhibits pronounced reactive variations, indicating an impedance mismatch. By introducing the F-shaped slot, the real part of the impedance is nearly 50 Ω at two resonant frequencies while the imaginary part approaches zero. So, the F-shaped slot not only introduces an additional resonant mode but also ensures proper impedance matching at the upper frequency of 5.67 GHz. This antenna behavior confirms that the F-shaped slot in the patch improves impedance matching and bandwidth.

3. Antenna Analysis with Frequency Selective Surface (FSS)

3.1. Design of FSS

The FSS structures are planner structures created by repeating unit cells and dimensions; the geometry and spacing between the cells determine the operating frequency of the FSS [34]. The geometry of the proposed unit cell is a double-arc, crossed, or butterfly-inspired structure. To obtain the proposed FSS structure, four-unit cells are placed in a row, and the row is repeated along the column, resulting in a 4×4 array. The hardware for the suggested antenna has also been fabricated. The geometric structure and hardware prototype of the designed FSS are

Accepted by Scientia Iranica

illustrated in Figures 7 (a) and (b). All the design parameters and their values are listed in Table 4. Unit cell size is 20 mm × 20 mm, while the size of the 4×4 array is 80 mm × 80 mm. The material used to design the FSS is the same as that used for the antenna, with a thickness of 0.8 mm. The edge-to-edge gap between the unit cells is 1 mm. The thickness of the FSS is also a critical parameter that needs to be analyzed for gain and efficiency enhancement, and the size of the FSS directly influences the resonance behavior [35]. The working principle of the frequency-selective surface is explained in [36], [37], [38].

This butterfly-shaped FSS geometry is selected to achieve a wideband response from 3.30 to 6.53 GHz. It is compact and has a single-layer structure. Various FSSs with conventional shapes, such as rectangular or square loops, and [39], ring structures, rectangular slotted, and fractal, star-shaped [40] or cross-shaped structures, generally having a complex structure or relying on a single or dual band with low bandwidth. In contrast, the proposed FSS supports a hybrid resonant response. This FSS does not require a multilayer or complex structure with a wideband response, which is rarely possible with a single-layer FSS.

The proposed FSS is also represented as an equivalent circuit model (ECM) in Advanced Design System (ADS), as shown in Figure 8. The ECM model of the FSS is a parallel combination of two series RLC circuits, and another parallel combination of L and C with R in series. The power dissipation in the copper creates resistance in the ECM. The values of the circuit components are summarized in Table 5 and were obtained using the fundamental equations (9)-(13).

$$Q = \frac{f_0}{\Delta f} \tag{9}$$

Δf is the 3 dB bandwidth, and f_0 is the resonant frequency of the circuit.

Capacitor value can be obtained using equation (10)

$$C = \frac{\varepsilon_0 \varepsilon_{eff} A}{g} \tag{10}$$

Where A is the area of the patch and g is the gap between unit cells. Similarly, L and R can be found using equations (11)-(13).

$$L = \frac{1}{(2\pi f_0)^2 C} \tag{11}$$

For a series circuit

Accepted by Scientia Iranica

$$R = \frac{\omega_0 L}{Q} \tag{12}$$

For a parallel circuit

$$R = Q\omega_0 L \tag{13}$$

The transmission and reflection coefficients of the suggested FSS, designed using HFSS and an equivalent circuit, are given in Figure 9(a), and the reflection phase of the FSS is shown in Figure 9(b). Results obtained from both the HFSS and the ECM are in good agreement.

Figure 10 shows the surface current distribution of the FSS unit cell at three different frequencies, 4, 5, and 6 GHz. As shown in Figure 10, strong currents are concentrated on the inner part of the crossed arms of the FSS. A small current is also distributed at the edges of the horizontal strip. This indicates a longer current path, which is mainly responsible for the lower resonance frequency, i.e. 4 GHz. At 5 GHz, the current is highly distributed over both crossed rectangular strips and the central circular connecting region. A small current is also distributed across the outer arcs and the horizontal strip, indicating strong coupling among multiple resonant paths. Again, at 6 GHz, the current distribution is more dominant and covers a larger portion of the crossed rectangular strips, the horizontal strip, and both the arc regions. Also, the current is concentrated in the central circular region, leading to higher-order resonant modes. Merging these adjacent resonant modes provides a wideband behavior. Additionally, this butterfly-shaped FSS increases the effective electrical length, thereby improving bandwidth without increasing size.

3.2. Integration of Antenna with FSS

To enhance the antenna gain, the suggested antenna is integrated with the designed FSS. The flowchart in Figure 11(a) describes the complete antenna design process. To enhance antenna gain with FSS, the phase of the reflected wave from the FSS must be in phase with the antenna radiation. The spacing between the antenna and the FSS is an essential parameter for generating a constructive interface between reflective waves from the FSS and the radiating waves from the antenna. Mathematically, the gap between the antenna and the FSS can be calculated using equation (14) [41], [42].

$$\varphi - 2\beta G = 2n\pi \tag{14}$$

Where n=….-1, 0, 1….

Accepted by Scientia Iranica

In equation (14), φ is the reflection phase, β is the free-space propagation constant, and n determines the resonance order of the cavity formed between the antenna and FSS. Generally, the spacing between the antenna and the FSS must be between 0.25λ and 0.5λ. For this antenna, the λ at the centre frequency of 4.95 GHz (3.44-6.45 GHz) is 60.6 mm, which lies within the cavity spacing range of λ/4 to λ/2. To achieve an optimal gap, several iterations were performed, and the optimised spacing between the antenna and the FSS was 22.2 mm, corresponding to 0.366λ. If the space is less than 22.2 mm, the antenna does not provide enough gain and good impedance matching. Increasing this gap increases the antenna's occupied space. Due to the wideband behaviour of the FSS, the spacing between the antenna and the FSS is optimized to maintain the antenna's wideband response while providing sufficient gain. So, a parametric optimization is performed for the spacing (H) between the antenna and FSS for a 4×4 element array. As the distance H decreases, it affects both the bandwidth and the reflection coefficients. For H = 18 mm, the reflection coefficients are above -12 dB. For H = 24 mm, the antenna maintains a wideband response, but the -10 dB Bandwidth shifts downwards. Hence, the antenna maintains a wideband response, good impedance matching, and sufficient gain for H = 22.2 mm. Thus, the FSS is placed below the antenna at a distance H = 22.2 mm, as optimized in HFSS through multiple iterations and the S-parameters for different values of H are shown in Figure 11(b). When this spacing is reduced to the near-field distance of around 10 mm, the antenna operates in the reactive near field. Strong electromagnetic coupling between the antenna and FSS alters the S-parameters, and the wideband response is not maintained with this spacing. So, an optimized spacing is selected to achieve a wideband response with gain enhancement.

From Figure 11(b), it is observed that the antenna exhibits a wideband response with a 22.2 mm gap. The antenna, integrated with FSS as simulated using HFSS, and a fabricated prototype are shown in Figures 12(a) and (b). The antenna and the FSS are separated by placing a foam of height H. S-parameters, gain, and other performance parameters of the antenna are explained in the next section.

4. Result Analysis of Antenna with and without FSS

This section of the paper discusses the different performance parameters of the antenna with and without the FSS integrated. These include S-parameters, gain, and radiation pattern. Additionally, the simulated and tested results are compared, and they match perfectly, except for minor discrepancies.

Accepted by Scientia Iranica

To verify the simulated results, a prototype of the developed antenna is fabricated. A prototype of the frequency-selective surface is also created. The experimental setup is illustrated in Figure 12(c). A Vector Network Analyzer with model number N9916A is used to measure the S-parameters. The S-parameters of the antenna alone and with the FSS integrated are shown in Figure 13.

This indicates that the antenna, without a frequency-selective surface, operates from 3.50 to 6.50 GHz, achieving a maximum return loss greater than -40 dB. When no FSS is placed, the antenna resonates at two frequencies, 5.7 and 3.95 GHz. The tested S-parameters also match the simulated values. After placing the frequency-selective surface, the lower -10 dB point shifts to a lower frequency, and the antenna operates from 3.18 to 6.35 GHz. The resonant frequencies in this case are 5.25 GHz and 3.5 GHz, with a maximum S11 value greater than -35 dB. This shift is due to the increase in electrical length caused by the FSS, which introduces an additional reactive load. Additionally, FSS alters the antenna's effective dielectric constant. From Figure 13, it can be seen that the simulated and measured results are in good agreement for both the antenna with and without FSS. The primary purpose of the antenna is to enhance its gain, which is necessary for 5G applications. For this, an FSS with a wideband response is designed and placed below the antenna. The gain of the antenna is plotted with and without FSS in Figures 14(a) and (b), respectively. Without FSS, the maximum gain of the antenna is around 4 dBi. After placing the FSS, the gain increases to 8.62 dBi, representing a 4.62 dBi improvement. From the figure, it is also observed that the gain improvement is not significant at higher frequencies, as it is at lower frequencies. This is because the design uses a FR-4 substrate. At high frequencies, dielectric losses may increase. So, at high frequency, the gain and efficiency may decrease. That’s why the gain decrement was observed.

The maximum gain achieved without integrating FSS is 4 dBi at 6 GHz. Figure 14(c) presents the simulated efficiency of the antenna with and without FSS. Without FSS, the computed efficiency exceeds 85%, reaching 87.94% across the entire operating frequency. With FSS, the antenna efficiency increased to 98.98%, with a minimum of 96%. There is a slight discrepancy between the computed and tested results, due to fabrication tolerances and the testing setup. An improvement in the antenna's front-to-back ratio (FBR) was also observed across the entire operating band after introducing the FSS below the antenna, as shown in Figure 14(d). The FBR without FSS is below 5 dB, indicating significant back radiation. After the introduction of FSS, the FBR improved, reaching more than 10 dB and fluctuating between 10 and 25 dB.

Accepted by Scientia Iranica

Antenna polarization is evaluated from the axial ratio. The axial-ratio plot in Figure 15 shows that it remains above 12 dB throughout the operating band. This confirms that the antenna is linearly polarized with no circularly polarized components. The radiation patterns of the antenna with and without FSS are plotted in Figure 16 for both E and H-planes. From Figure 16, the radiation pattern without FSS is observed to be omnidirectional. After integrating FSS, the radiation patterns in both the E and H planes are directional, with reduced back lobes, resulting in increased gain, which is desirable for 5G wireless communication in the sub-6 GHz band. The 3D gain plots of the antenna without FSS and with FSS integrated are shown in Figure 17, confirming that the maximum gain with FSS is 8.2 dBi at 4 GHz.

To verify the suitability of the antenna for the mentioned applications, the suggested antenna integrated with FSS is compared with related work carried out in the literature listed in Table 6. Integration of the FSS with the antenna improved its gain and directivity. The antenna is compared in terms of size, FSS, frequency range, and gain with and without FSS. The antennas in [43] and [44] are large and have lower gain than the proposed antenna. The antennas do not use an FSS but are large and achieve a maximum gain of 5.58 dBi. Additionally, the gain and operating frequency range are lower than those of the proposed antenna. The dimensions of the antenna and FSS are smaller than those of the proposed antenna and FSS in some of the references, as shown in Table 6. However, the frequency range is 3.5-5.4 GHz, which is lower than that of the antenna developed in this paper. FSS can be employed in MIMO antennas. One of the antennas used an FSS to enhance gain. FSS size is larger than the proposed antenna, and the gain is also less than that of the proposed antenna, which is 7.6 dBi. The antenna in [44], do not use FSS; the size is large, and the operating bandwidths and gains are smaller. Similarly, one of the antennas is a two-port antenna with a low gain of 4 dBi. The proposed antenna is also superior to [45] and [46] in terms of size, gain, and bandwidth. The proposed antenna also ensures a high efficiency of above 98%. Additionally, the proposed FSS is a single-layer FSS with a simple structure. There is no additional requirement for the enhancement of gain via such a means or any other electronic components. The antenna is also better than the other antennas, as listed in Table 6. This analysis demonstrates that the proposed antenna outperforms the reported antennas in the literature.

5. Conclusion

An antenna with high gain and wideband response is designed and tested in this paper. Gain enhancement is achieved using an FSS. The geometry of the antenna is simple with a modified elliptical F-slotted patch and a slotted partial ground plane. An increase of approximately 4 dBi

Accepted by Scientia Iranica

in gain is achieved with the FSS. The antenna is small, measuring 22 mm × 29 mm, and is constructed from FR-4 with a thickness of 0.8 mm. FSS size is 80 mm × 80 mm, designed on the same material, i.e., FR-4 with the same thickness. The antenna operates over a wide frequency range, from 3.5 to 6.5 GHz with FSS and from 3.18 to 6.35 GHz without FSS, with appropriate reflection coefficients. The antenna's wideband response covers the sub-6 GHz band used for 5G services. Without FSS, the gain is 4.65 dBi, while it increases to 8.62 dBi using FSS. The proposed antenna is compared with recently reported antennas and found to be superior. This antenna covers several 5G sub-6 GHz bands, including n46 (5.15 – 5.925 GHz), n47 (5.855 – 5.925 GHz), n48 (3.550 – 3.700 GHz), n77 (3.30 – 4.20 GHz), n78 (3.30 – 3.80 GHz), n79 (4.40 – 5.0 GHz), and n102 (5.925 – 6.425 GHz). Additionally, the antenna supports other wireless services, including Wi-Fi (5/6/6E), WiMAX, the ISM band at 5.8 GHz, and the public safety band at 4.9 GHz.

Acknowledgment

The authors would like to thank Jaipur National University, Jaipur, and Parul University, Vadodara, for providing facilities to conduct this research, and Charotar University of Science and Technology (CHARUSAT), Anand, Gujarat, for the measurement.

Author Contributions: Chandra Shekhar Rajora: Conceptualization, Simulation, Formal Analysis, Investigation, Methodology, Software, Validation, Writing – original draft; **Prem Pal Singh:** Result Analysis, Investigation, Project administration, Software, Supervision, Visualization, Writing – review & editing; **Sudhir Kumar Sharma:** Investigation, Resources, Validation, Writing – review & editing

Disclosure

All authors have read and approved the final version of the manuscript for publication.

Abbreviations: FSS: Frequency Selective Surface, **VNA:** Vector Network Analyzer, **Wi-Fi**: Wireless Fidelity, **WiMAX**: Worldwide Interoperability for Microwave Access, **ADS**: Advanced Design System, EBG: Electromagnetic Band Gap Structure, AMC: Artificial Magnetic Conductor

References:

Accepted by Scientia Iranica

[1] Dhananjeyan, R., Pant, M., Vishalatchi, K., et al. “High-performance Compact Antenna for Sub-6 GHz 5G MIMO Applications,” Progress In Electromagnetics Research C, 157(1), pp. 57–63, (2025). https://doi.org/10.2528/PIERC25051001.

[2] Kiani, S., Rezaei, P., and Fakhr, M. “On-chip coronavirus shape antenna for wide band applications in terahertz band,” Journal of Optics (India), 52(2), pp. 860–867, (2023). https://doi.org/10.1007/s12596-022-01048-y.

[3] Kiani, S., Rezaei, P., and Fakhr, M. “A CPW-fed wearable antenna at ISM band for biomedical and WBAN applications,” Wireless Networks, 27(1), pp. 735–745, (2021). https://doi.org/10.1007/s11276-020-02490-1.

[4] Keshwala, U., Rawat, S., and Ray, K. “Circularly polarized truncated corner square slot antenna for Ku-band applications,” Scientia Iranica, 30(1D), pp. 218–227, (2023). https://doi.org/10.24200/sci.2021.57467.5255.

[5] Tseng, D. “Spectrum for 4G and 5G: Global Update on 5G Spectrum Presentation,” (2019).

[6] Khan, R., Sethi, W., Malik, W., et al. “Enhancing gain and isolation of a quad-element MIMO antenna array design for 5G sub-6 GHz applications assisted with characteristic mode analysis,” Scientific Reports, 14(1), (2024). https://doi.org/10.1038/s41598-024-61789-7.

[7] Mohsin, N.K., and Naji, D.K. “Design of a Compact Sub-6 GHz Wideband Filtering Patch Antenna without Extra Structure,” Progress in Electromagnetics Research C, 155, pp. 165–175, (2025). https://doi.org/10.2528/PIERC25013002.

[8] Kumar, A., De, A., and Jain, R.K. “Gain Enhancement Using Modified Circular Loop FSS Loaded with Slot Antenna for Sub-6 GHz 5G Application,” Progress In Electromagnetics Research Letters, 98, pp. 41–48, (2021). https://doi.org/10.2528/PIERL21031108.

[9] Ambika, A., Sivashanmugavalli, and Parthiban, N., et al. “A FSS Loaded High Gain Semi-Circle Monopole Antenna for 5G Applications,” Journal of Nano- and Electronic Physics, 16(4), (2024). https://doi.org/10.21272/jnep.16(4).04038.

[10] Rai, V.K., and Kumar, M. “Novel Dual-Band Frequency Selective Surface and its Applications on the Gain Improvements of Compact UWB Monopole Antenna,” Defence Science Journal, 73(5), pp. 582–593, (2023). https://doi.org/10.14429/dsj.73.5.18684.

[11] Raj, T., Mishra, R., Kumar, P., et al. “Design and Development of a FSS backed High Gain UWB MIMO Planar Antenna for FR-II NR Bands,” Results in Engineering, 26, pp. 105034, (2025). https://doi.org/10.1016/j.rineng.2025.105034.

[12] Arif, B., Bilal, M., Quddus, A., et al. “A Split Center Resonator FSS-Based Gain Enhancement of CPW Feed UWB Antenna for High Gain UWB Communication,” IEEE Access, 12(1), pp. 73247–73257, (2024).https://doi.org/10.1109/ACCESS.2024.3403719.

[13] Aishwarya, T., and Das, P. “A FSS integrated wearable modified bow-tie antenna for biomedical applications,” Results in Engineering, 26, (2025). https://doi.org/10.1016/j.rineng.2025.104894.

[14] Keshwala, U., Rawat, S., and Ray, K. “Half hexagonal shaped UWB antenna with triple band notch using resonating structures for wireless communication,” Scientia

Accepted by Scientia Iranica

Iranica, 31(17), pp. 1547–1555, (2024). https://doi.org/10.24200/sci.2023.59268.6145.

[15] Suvalka, R., Agrahari, S., Yadav, A.K.S., et al. "EBG and SRR loaded triple band notched UWB antenna," Scientia Iranica, 31(5), pp. 458–468, (2024). https://doi.org/10.24200/sci.2022.59023.6032.

[16] Fernandes, E.M.F., Silva, M.W.B., Briggs, L.S., et al. "2.4–5.8 GHz dual-band patch antenna with FSS reflector for radiation parameters enhancement," AEU - International Journal of Electronics and Communications, 108, pp. 235–241, (2019). https://doi.org/10.1016/j.aeue.2019.06.021.

[17] Verulkar, S., Rochkari, A., Trimukhe, M., et al. "High Gain Compact Dual Band Antenna Using Frequency Selective Surface for 5G and WLAN Applications," Progress In Electromagnetics Research C, 142, pp. 1–11, (2024). https://doi.org/10.2528/PIERC24010101.

[18] Abhilash, A.P., Indhu, K.K., Anilkumar, R., et al. "Frequency Selective Surface (FSS) Loaded, CPWfed, MIMO antenna with Wider Bandwidth and Enhanced Gain for sub 6 GHz 5G Applications," in 2022 International Conference on Futuristic Technologies, INCOFT 2022, Institute of Electrical and Electronics Engineers Inc., (2022). https://doi.org/10.1109/INCOFT55651.2022.10094406.

[19] Sharma, S., Singh, D., Särestöniemi, M., et al. "On-body FSS-backed High Gain Microwave System for Brain Tumor Diagnosis," Progress In Electromagnetics Research C, 155, pp. 245–254, (2025). https://doi.org/10.2528/PIERC25022103.

[20] Keshwala, U., Ray, K., and Rawat, S. "Honeycomb shaped fractal antenna with dual notch characteristic for UWB applications," Scientia Iranica, 29(6D), pp. 3338–3346, (2022). https://doi.org/10.24200/SCI.2021.56585.4799.

[21] Sharma, A., Khah, S.K., and Rawat, S. "Compact Y-shaped antenna with partial and meandered ground for WLAN/Wi-MAX applications," Scientia Iranica, 31(17), pp. 1556–1566, (2024). https://doi.org/10.24200/sci.2022.59299.6163.

[22] Attioui, S., Khabba, A., Ibnyaich, S., et al. "Design of a Miniaturized Circular Flower-Shaped Fractal Antenna with a Defected Ground Structure for Multiband Applications," Progress in Electromagnetics Research C, 155, pp. 203–211, (2025). https://doi.org/10.2528/PIERC25022001.

[23] Albaihani, Y., Akram, R., Almohaimeed, A.M., et al. "Miniaturized EBG Antenna for Efficient 5.8 GHz RF Energy Harvesting in Self-Powered IoT and Medical Sensors," Sensors, 25(15), (2025). https://doi.org/10.3390/s25154777.

[24] Renit, C., and Raj, T.A.B. "Wearable frequency selective surface-based compact dual-band antenna for 5G and Wi-Fi applications," Automatika, 65(2), pp. 454–462, (2024). https://doi.org/10.1080/00051144.2023.2296796.

[25] Maged, R., El-Hameed, A.S.A., Mabrook, M.M., et al. "Enhanced performance of microstrip antenna fabricated on a composite dielectric substrate coupled with multiple dielectric superstrates," Optical and Quantum Electronics, 56(5), (2024). https://doi.org/10.1007/s11082-024-06487-4.

[26] Kiani, S.H., Alharbi, A.G., Khan, S., et al. "Wideband Three Loop Element Antenna Array for Future 5G mmwave Devices," IEEE Access, 10, pp. 22472–22479, (2022). https://doi.org/10.1109/ACCESS.2022.3152769.

Accepted by Scientia Iranica

[27] Megahed, A.A., Hussein, A.H., Al-Gburi, A.J.A., et al. “Compact Wideband Antenna Array with DGS-Based Metamaterial for Efficient Smartphone Communication and SAR Reduction,” Progress in Electromagnetics Research B, 110, pp. 15–28, (2025). https://doi.org/10.2528/PIERB24120504.

[28] Dokmetas, B., Arican, G.O., Akcam, N., et al. “A novel millimeter-wave U-shaped radiating slot antenna with DGS structures for 5G cellular application,” in 2019 11th International Conference on Electrical and Electronics Engineering (ELECO), IEEE, pp. 669–672, (2019). https://doi.org/10.23919/ELECO47770.2019.8990502.

[29] Rawal, P., and Rawat, S. “A frequency and polarization reconfigurable L-shaped patch antenna with defected ground structure,” Scientia Iranica, 30(5D), pp. 1703–1713, (2023). https://doi.org/10.24200/sci.2021.57874.5451.

[30] Pandey, R., Biswas, A.K., and Chakraborty, U. “Compact body-worn MIMO antenna with high port isolation for UWB applications,” International Journal of Communication Systems, 37(9), (2024). https://doi.org/10.1002/dac.5764.

[31] Tiwari, R.N., Sharma, D., Singh, P., et al. “Triple band lateral 4-port flexible MIMO antenna for millimeter wave applications at 24/28/38 GHz,” Results in Engineering, 26, (2025). https://doi.org/10.1016/j.rineng.2025.104678.

[32] “Ellipse,” Wolfram MathWorld. https://mathworld.wolfram.com/Ellipse.html.

[33] Balanis, C.A. Antenna Theory: Analysis and Design, 3rd ed., Wiley Interscience, (2005).

[34] Zeain, M.Y., Abu, M., Althuwaybi, A.A., et al. “A New Technique of FSS-Based Novel Chair-Shaped Compact MIMO Antenna to Enhance the Gain for Sub-6GHz 5G Applications,” IEEE Access, 12, pp. 49489–49507, (2024). https://doi.org/10.1109/ACCESS.2024.3380013.

[35] Dokmetas, B., Shinde, S.S., and Belen, M.A. “Artificial Intelligence Based Deep Learning Surrogate Model for Design Optimization of Microstrip Frequency Selective Surface,” in 2024 International Conference on Emerging Smart Computing and Informatics, ESCI 2024, Institute of Electrical and Electronics Engineers Inc., (2024). https://doi.org/10.1109/ESCI59607.2024.10497238.

[36] Kapoor, A., Kumar, P., and Mishra, R. “Analysis and design of a passive spatial filter for sub-6 GHz 5G communication systems,” Journal of Computational Electronics, 20(5), pp. 1900–1915, (2021). https://doi.org/10.1007/s10825-021-01742-3.

[37] Anwar, R., Mao, L., and Ning, H. “Frequency Selective Surfaces: A Review,” Applied Sciences, 8(9), pp. 1689, (2018). https://doi.org/10.3390/app8091689.

[38] Ünaldı, S., and Teşneli, N.B. “A closely spaced dual band polarization insensitive FSS for 5G applications,” Optik, 315, pp. 172040, (2024). https://doi.org/10.1016/j.ijleo.2024.172040.Ainthachot, C., Janpangngern, P., Dentri, S., et al. “Investigations of a Circularly Polarized Slotted Corner-Truncated Microstrip Patch Antenna with Split-Ring AMC Reflector,” in 2025 13th International Electrical Engineering Congress (iEECON), IEEE, pp. 1–5, (2025). https://doi.org/10.1109/iEECON64081.2025.10987871.

[39] Ainthachot C, Janpangngern P, Dentri S, et al., “Investigations of a Circularly Polarized Slotted Corner-Truncated Microstrip Patch Antenna with Split-Ring AMC

Accepted by Scientia Iranica

Reflector," in *2025 13th International Electrical Engineering Congress (iEECON)*, IEEE, Mar. 2025, pp. 1–5. doi: 10.1109/iEECON64081.2025.10987871.

[40] Rayan, R.R., Tabassum, T., Rahman, A., et al. "Design of a compact dual band antenna with novel FSS for enhanced gain in X-band applications," Results in Engineering, 26, pp. 105418, (2025). https://doi.org/10.1016/j.rineng.2025.105418.

[41] Hussain, M., Sufian, M.A., Alzaidi, M.S., et al. "Bandwidth and Gain Enhancement of a CPW Antenna Using Frequency Selective Surface for UWB Applications," Micromachines, 14(3), (2023). https://doi.org/10.3390/mi14030591.

[42] Deshmukh, A.A., Nawale, S.D., Kapure, V.R., et al. "Highly Isolated Compact Dual-Band MIMO Antenna Using Stubs, Slots and Neutralization Line for 5G Wi-MAX and WLAN Applications," Progress In Electromagnetics Research C, 158, pp. 27–35, (2025). https://doi.org/10.2528/PIERC25051801.

[43] Prajapati, B.D., Jaiswal, B., and Dalvadi, P.J. "Wideband Antenna Design with Notched Flower Shaped Patch for Wireless Applications," Progress In Electromagnetics Research C, 158, pp. 1–8, (2025). https://doi.org/10.2528/PIERC25061101.

[44] Boularas, A., Flissi, M., Rouabah, K., et al. "Improved Gain of a Compact Slot Antenna using an FSS Reflector for GNSS L1/E1/B1/G1 Bands," Radioengineering, 33(4), pp. 733–743, (2024). https://doi.org/10.13164/RE.2024.0733.

[45] Troudi, I., Baccouch, C., Chibani, B., et al. "Integration of frequency selective surfaces with MIMO antennas for enhanced performance in IoT and V2V communication systems," Scientific Reports, 15(1), (2025). https://doi.org/10.1038/s41598-025-19483-9.

[46] Troudi, I., Baccouch, C., and Chibani, R.B. "Design and enhancement of microstrip patch antenna with frequency selective surface backing for vehicle-to-vehicle communication," International Journal of Electrical and Computer Engineering, 14(6), pp. 6445–6454, (2024). https://doi.org/10.11591/ijece.v14i6.pp6445-6454.

Accepted by Scientia Iranica

Figures Captions List

Figure 1. Geometry of the Antenna (a) Front View (b) Back View (c) Fabricated Prototype

Figure 2. (a) Equivalent Circuit of the Suggested Antenna, (b) S-Parameters of Circuit and HFSS

Figure 3. Design Evolution Steps of the Designed Antenna

Figure 4. S-Parameters for Different Steps

Figure 5. Parametric Analysis of the Antenna (Variation in S-Parameters and bandwidth with W_1, W_2, W_4, L_g)

Figure 6. Surface Current Distribution with F-shaped slot at (a) 4 GHz, (b) 5 GHz, (c) 6 GHz (d) Surface current distribution without F-shaped slot at 4, 5 and 6 GHz (e) S-Parameters of Antenna without F-shaped slot (f) Simulated Impedances of the proposed antenna with and without F-Slot

Figure 7. (a) Geometric layout of the Proposed FSS (b) Fabricated Prototype of FSS

Table Captions List

Accepted by Scientia Iranica

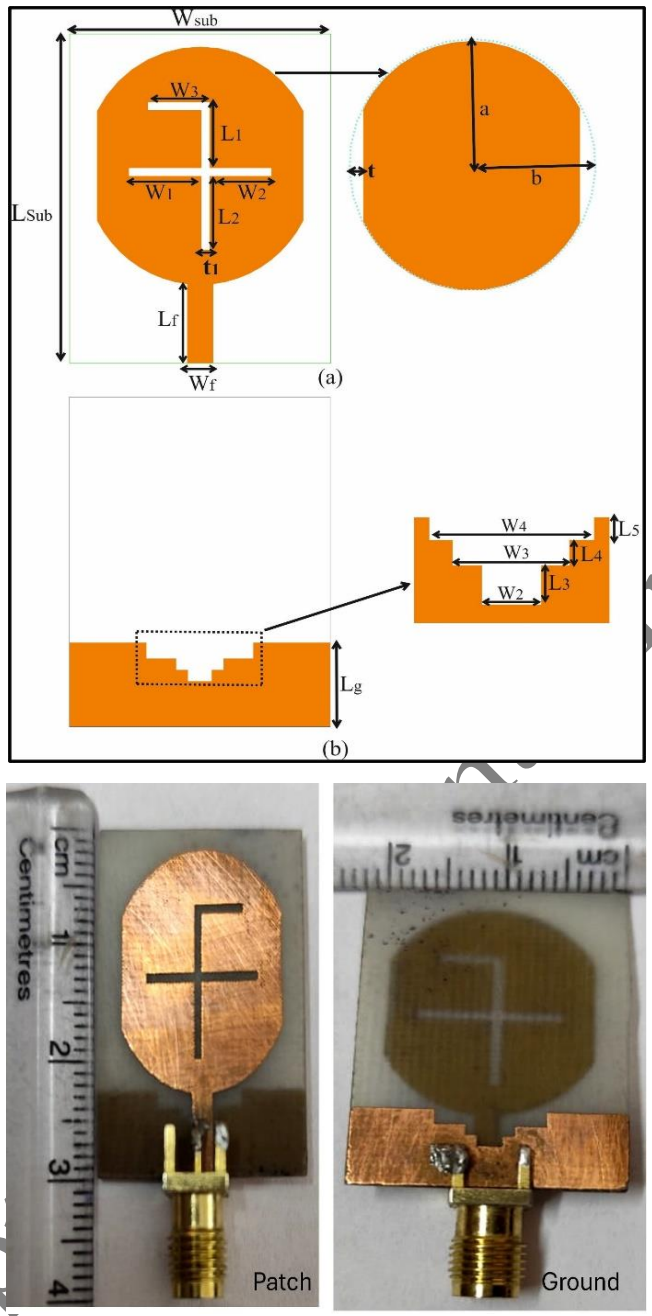

Figure 1. Geometry of the Antenna (a) Front View (b) Back View (c) Fabricated Prototype

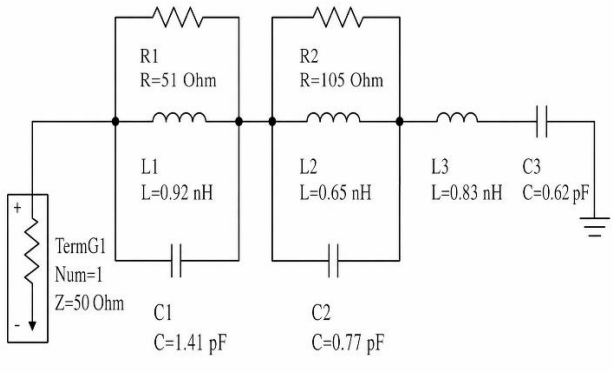

(a)

Accepted manuscript

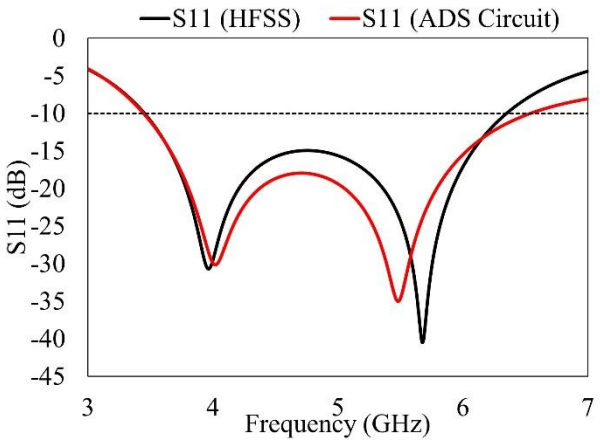

(b)

Figure 2. (a) Equivalent Circuit of the Suggested Antenna, (b) S-Parameters of Circuit and HFSS

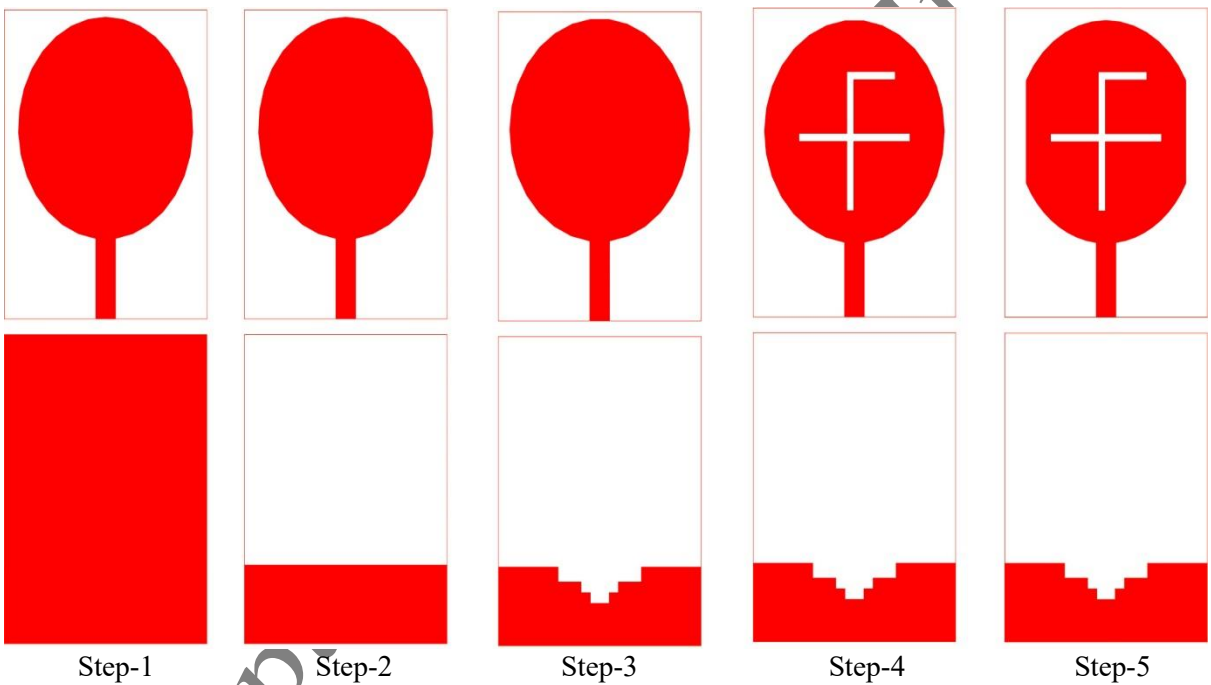

Figure 3. Design Evolution Steps of the Designed Antenna

Accepted Manuscript

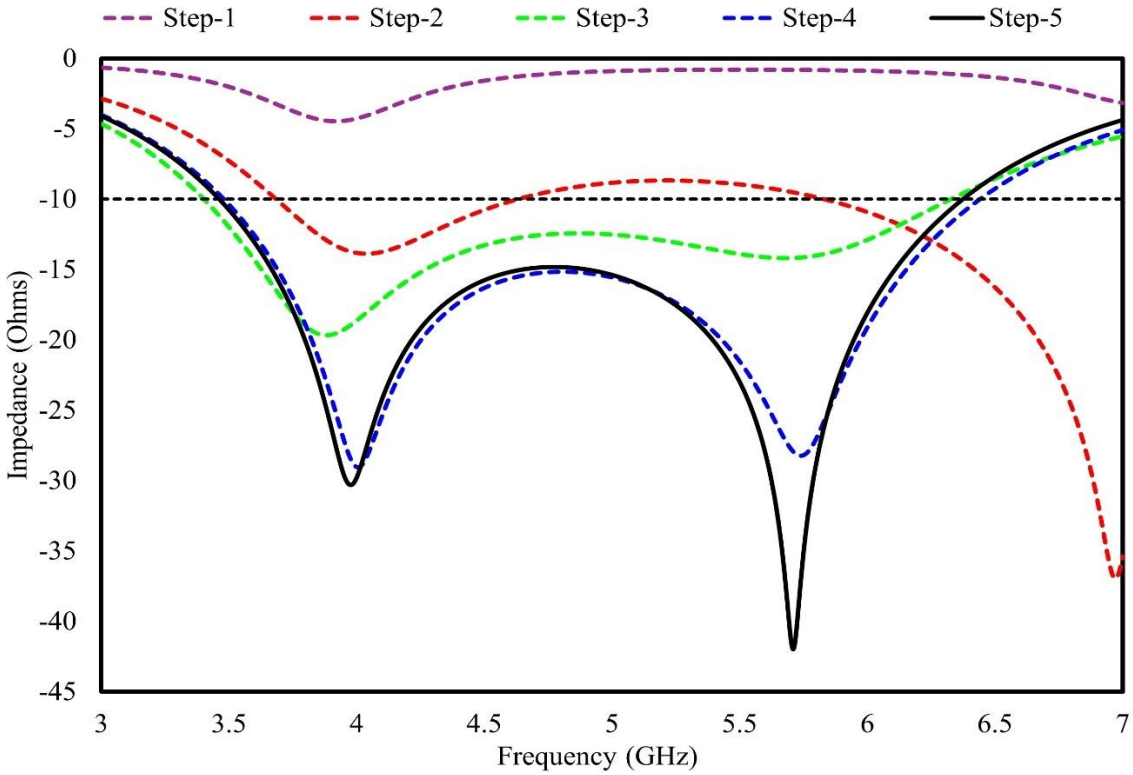

Figure 4. S-Parameters for Different Steps

Accepted by Scientific

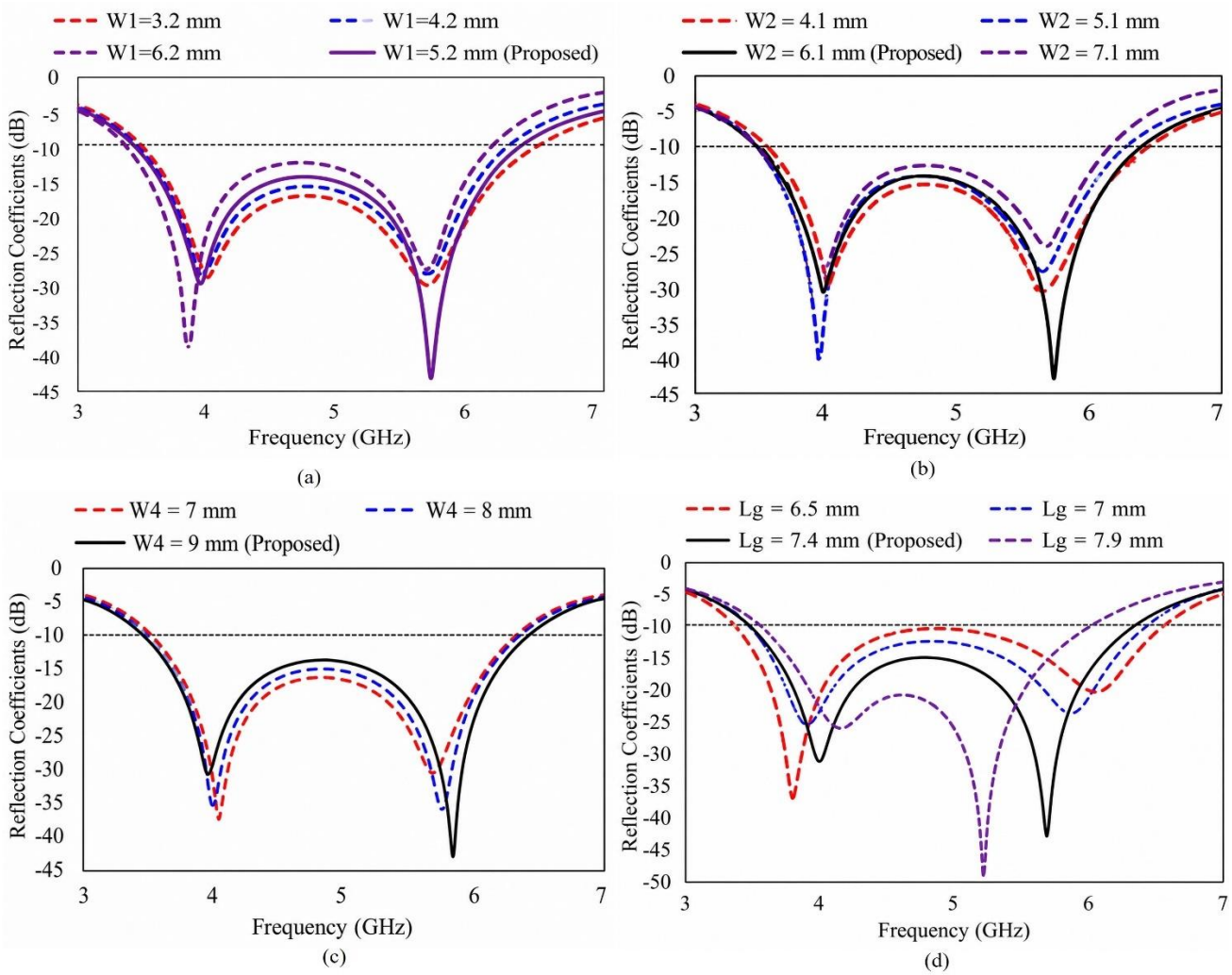

Figure 5. Parametric Analysis of the Antenna (Variation in S-Parameters and bandwidth with W_1, W_2, W_4, L_g)

Accepted by

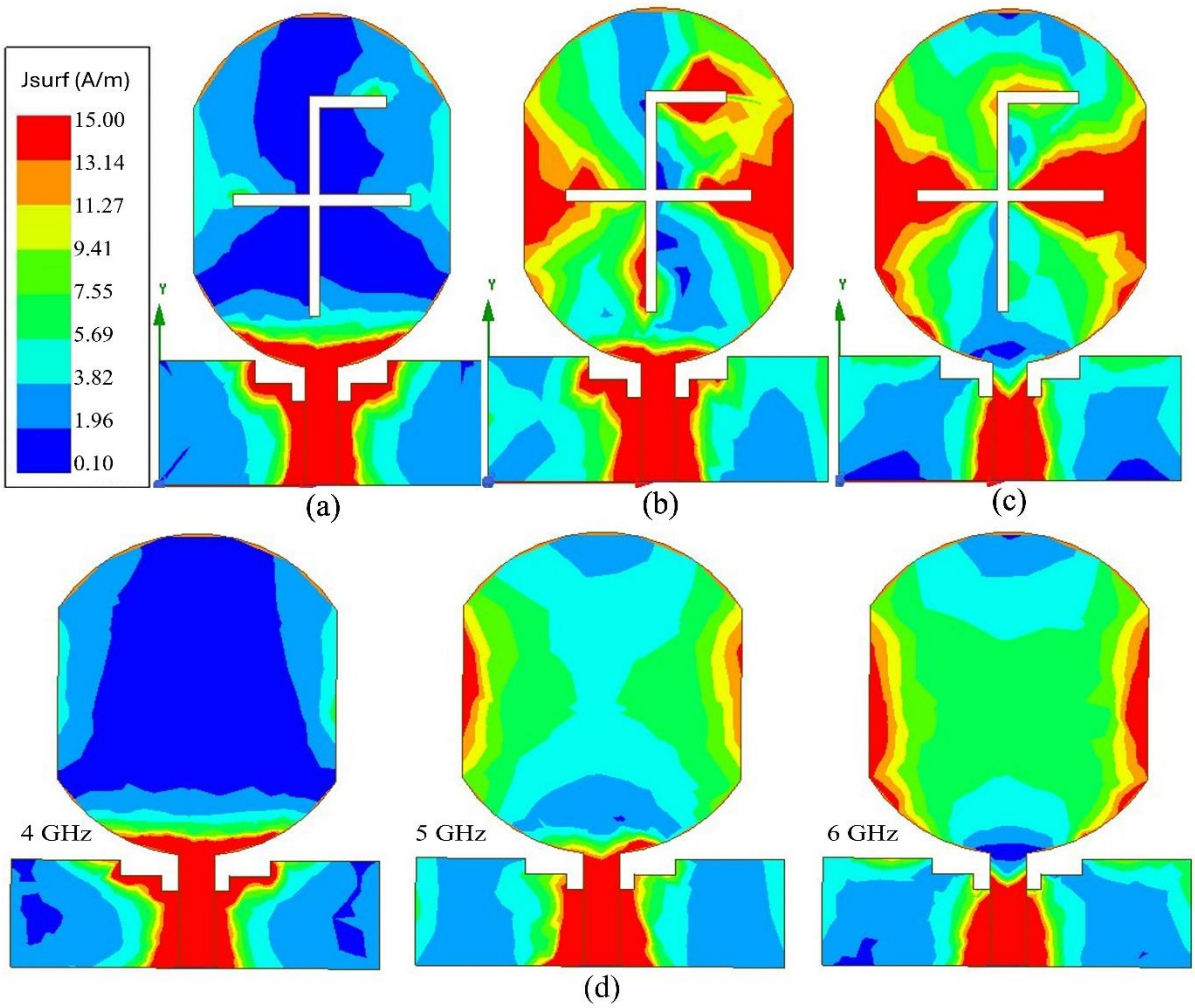
Jsurf (A/m)
15.00
13.14
11.27
9.41
7.55
5.69
3.82
1.96
0.10
(a)
(b)
(c)
4 GHz
5 GHz
6 GHz
(d)

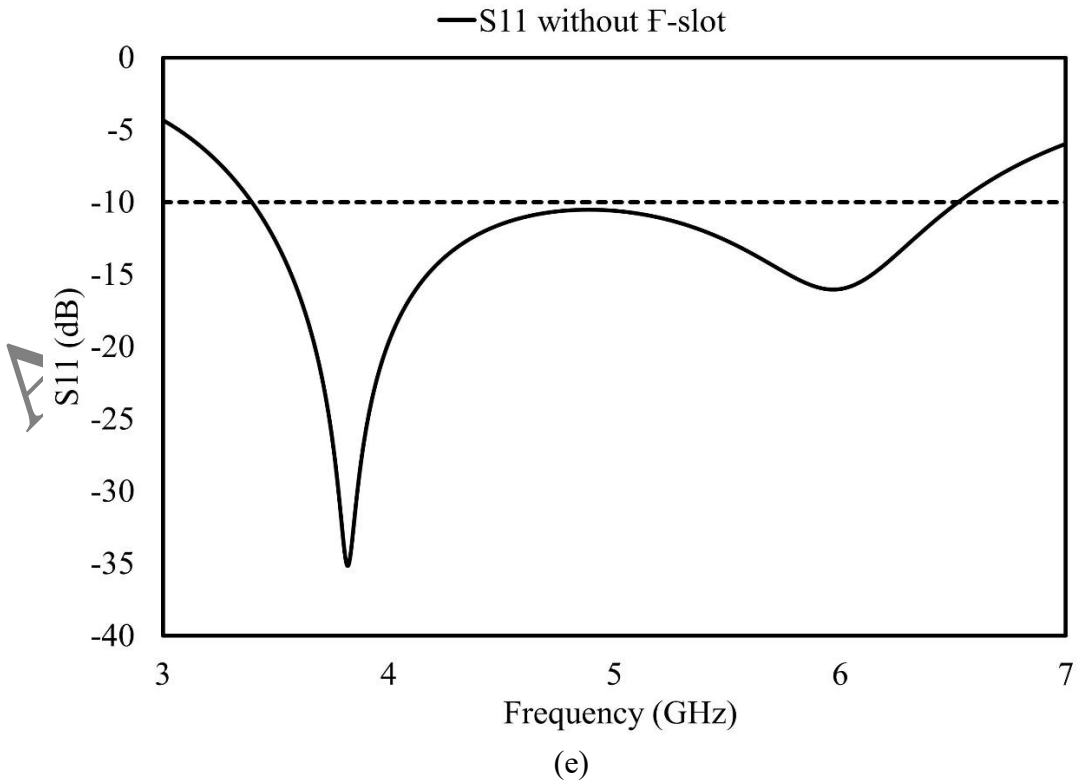
S11 without F-slot
0
-5
-10
-15
-20
-25
-30
-35
-40
S11 (dB)
3
4
5
6
7
Frequency (GHz)
(e)

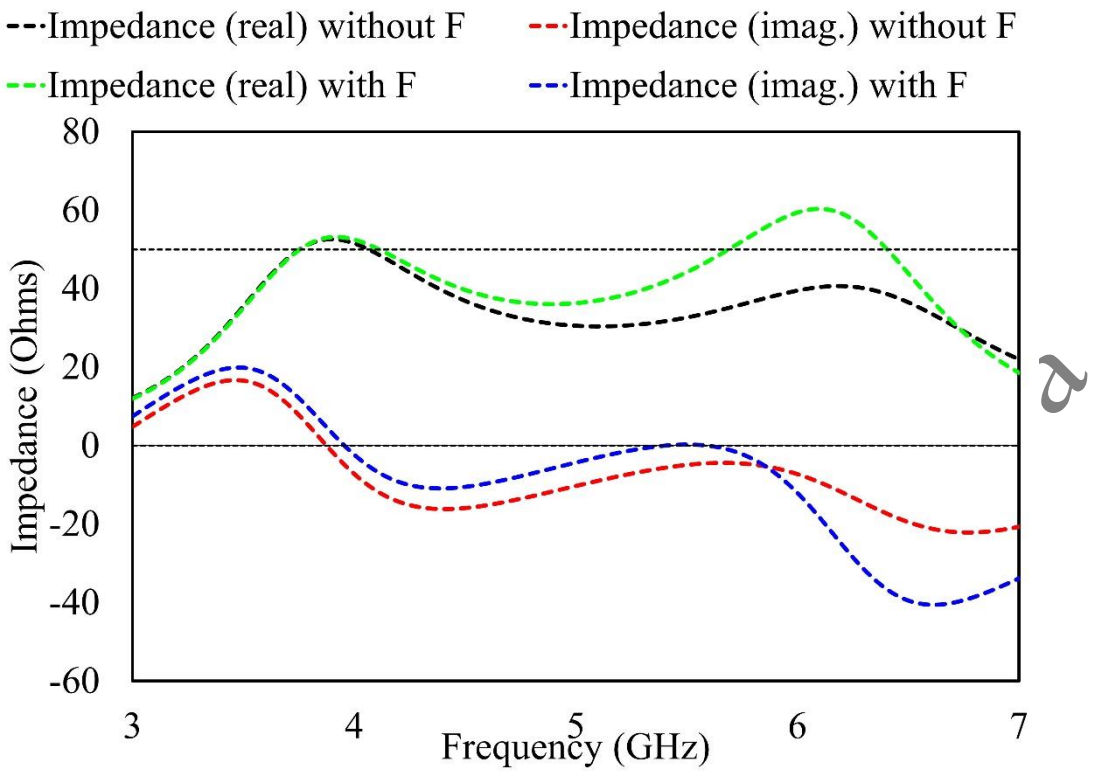

Figure 6. Surface Current Distribution with F-shaped slot at (a) 4 GHz, (b) 5 GHz, (c) 6 GHz (d) Surface current distribution without F-shaped slot at 4, 5 and 6 GHz (e) S-Parameters of Antenna without F-shaped slot (f) Simulated Impedances of the proposed antenna with and without F-Slot

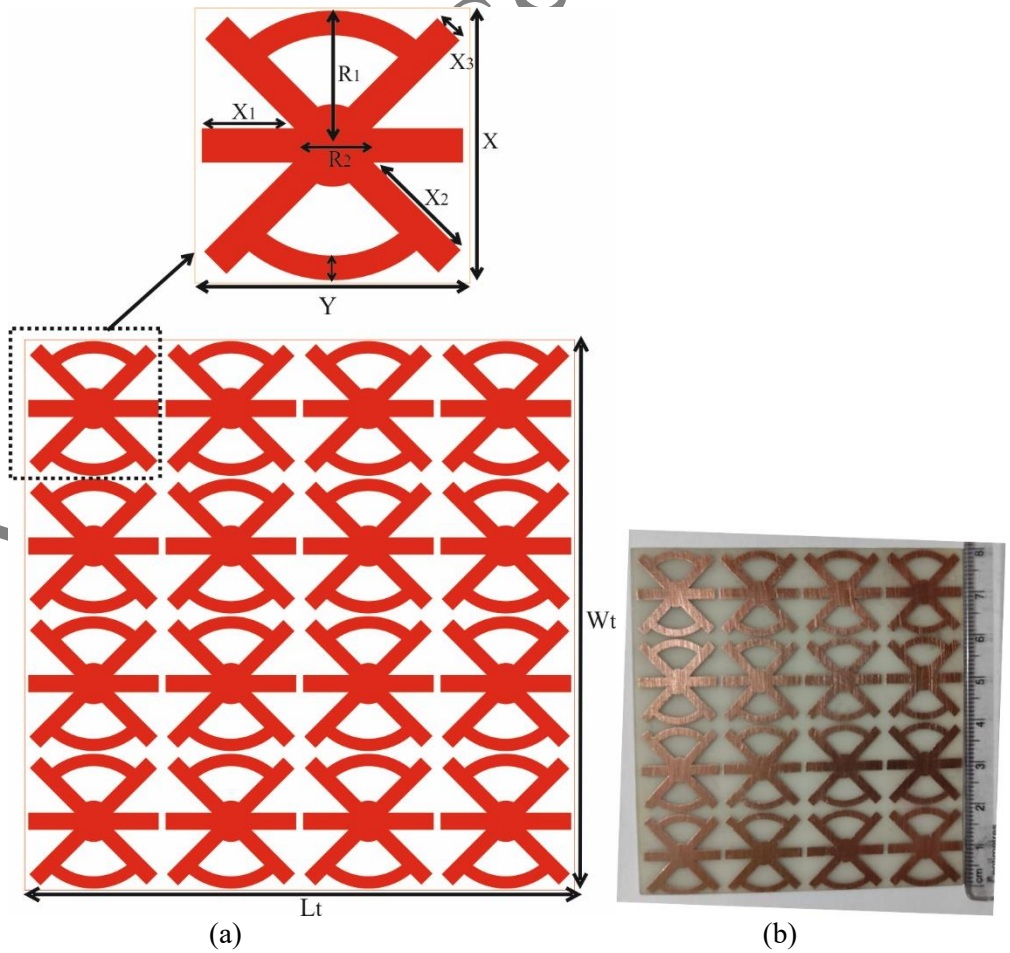

Figure 7. (a) Geometric layout of the Proposed FSS (b) Fabricated Prototype of FSS

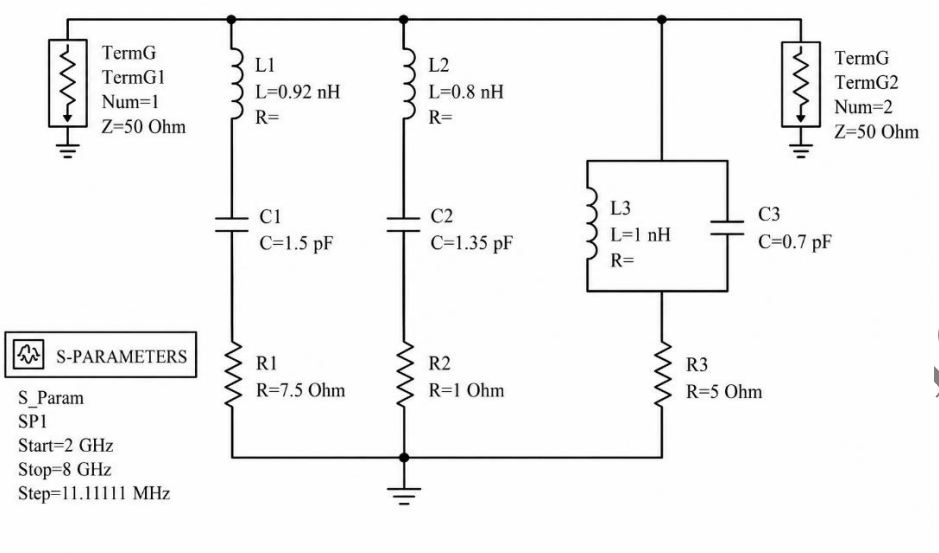

Figure 8. Equivalent Circuit of Proposed Frequency-Selective Surface

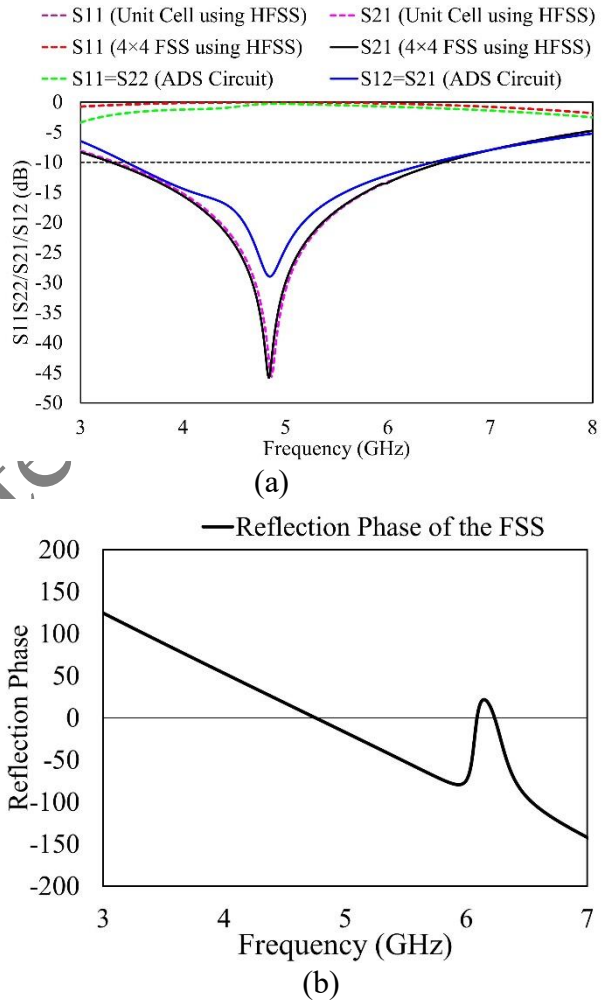

Figure 9. S-Parameters of the Designed FSS (HFSS and Equivalent Circuit in ADS) (b) Reflection phase of the designed FSS

Accepted

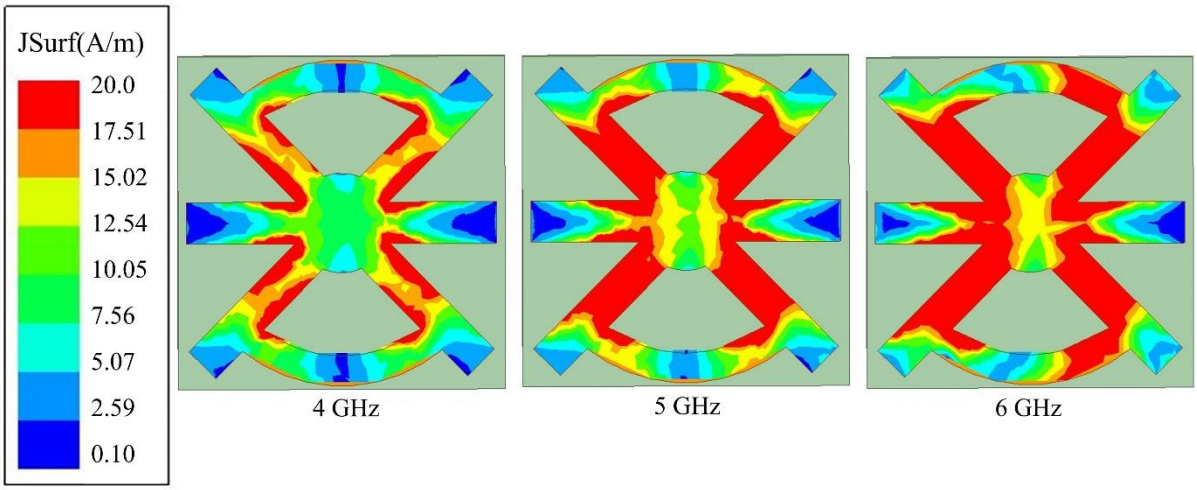

Figure 10. Surface current distribution of the FSS unit cell at 4, 5, and 6 GHz

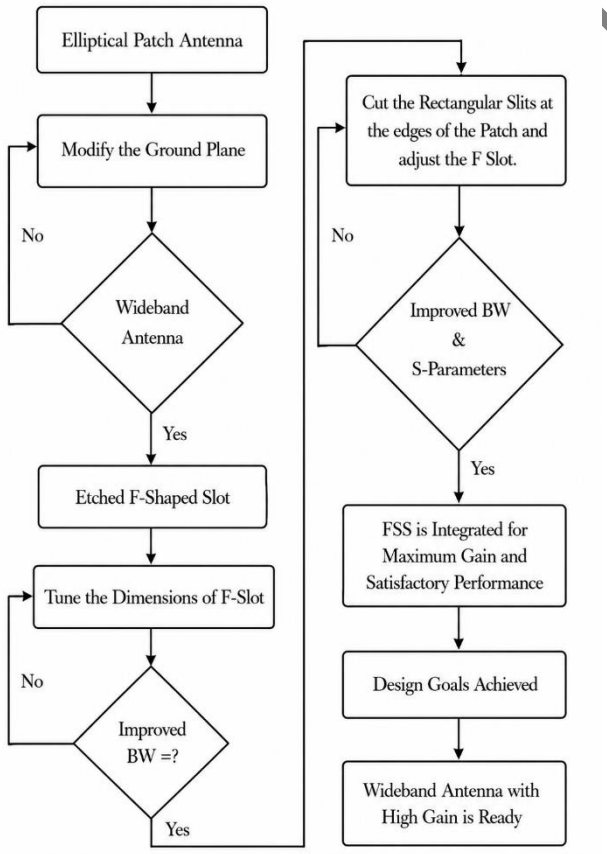

(a)

Accept

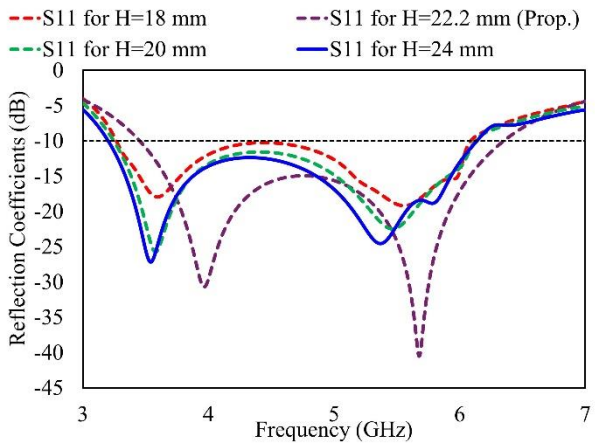

(b)

Figure 11. (a) Flow chart of the complete antenna design process (b) S-Parameters of the Antenna with FSS for different spacing between antenna and FSS

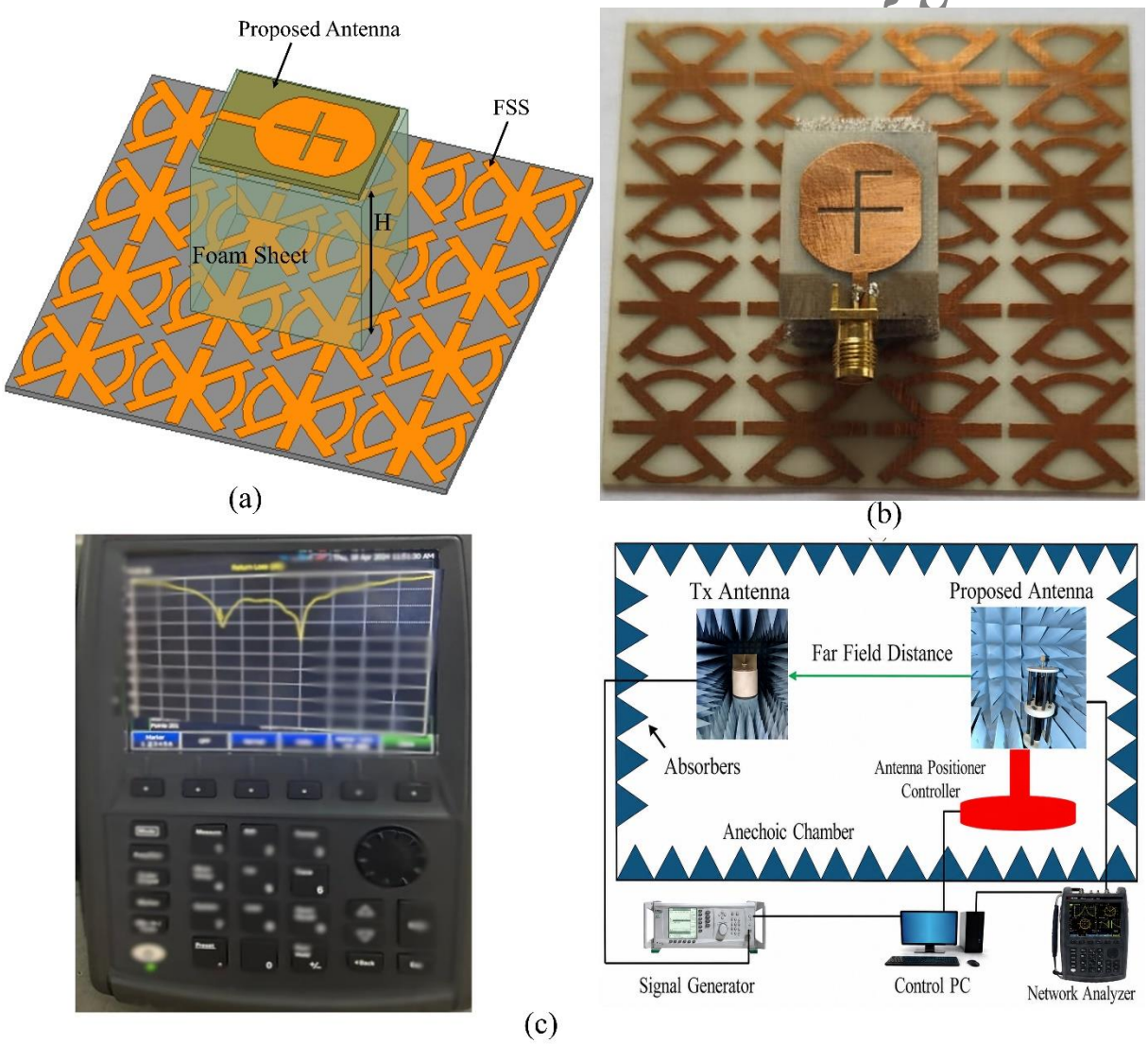

Figure 12. (a) Antenna with FSS (b) Fabricated FSS (c) Measurement setup

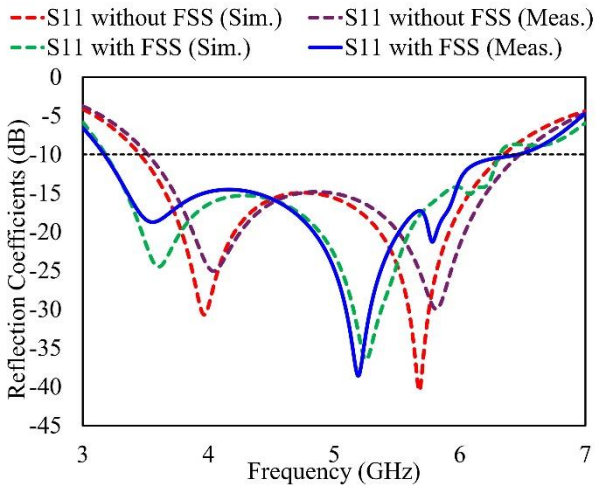

Figure 13. S-Parameters of the Antenna with and without FSS

Iranica

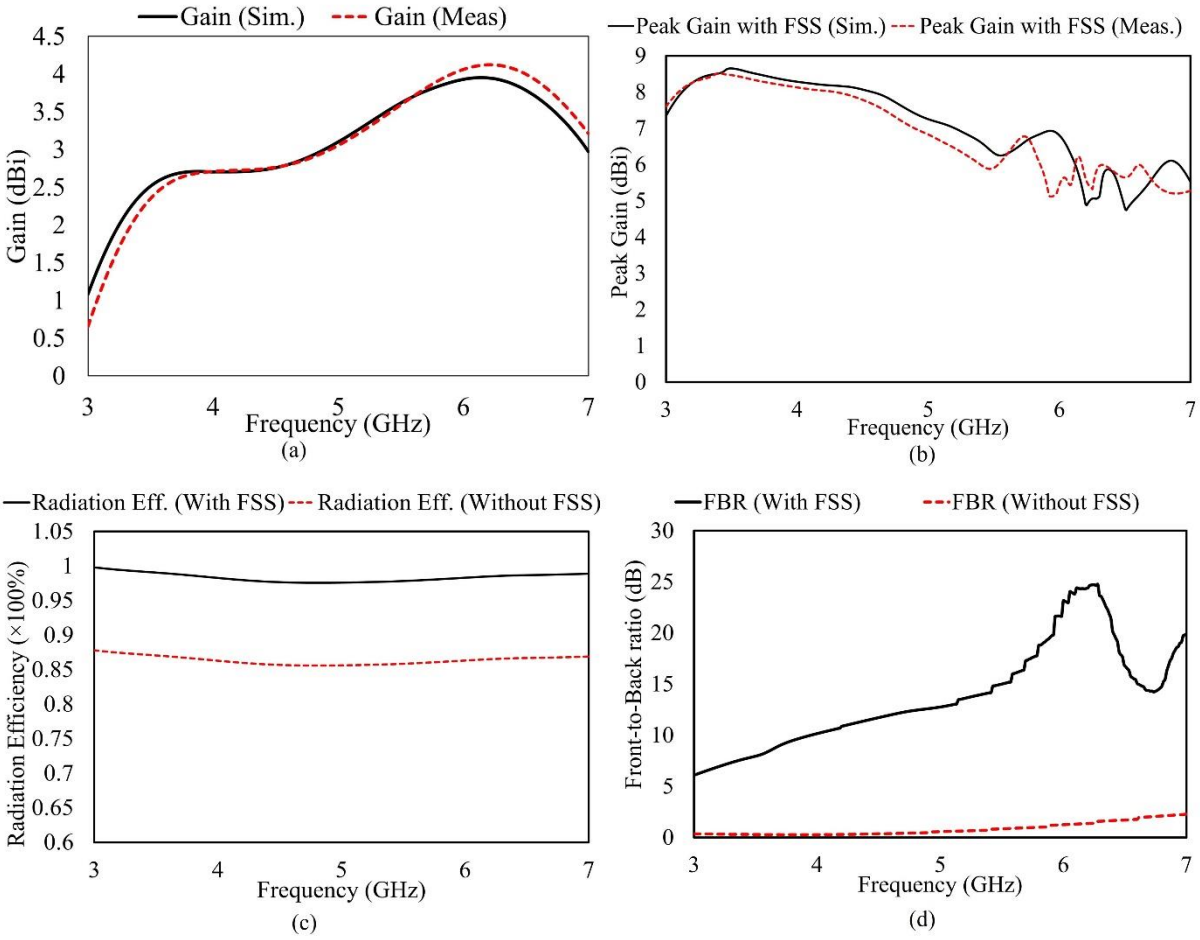

Figure 14 Computed and Tested Gain (a) Without FSS (b)With FSS. (c) Radiation Efficiency with and without FSS (d) Front-to-Back Ratio

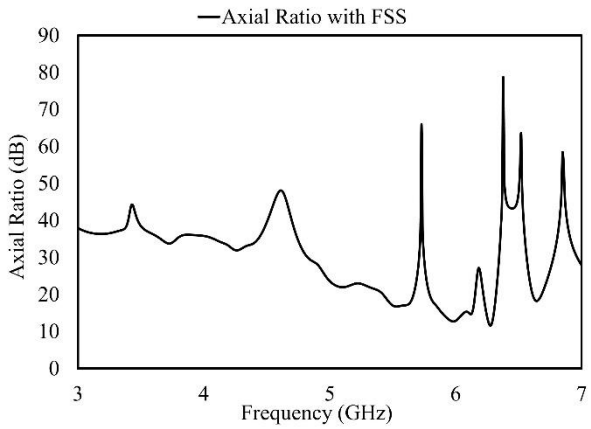

Figure 15. Axial Ratio of the Proposed Antenna confirms that the antenna is linearly polarized

Accepted by Scientia Iranica

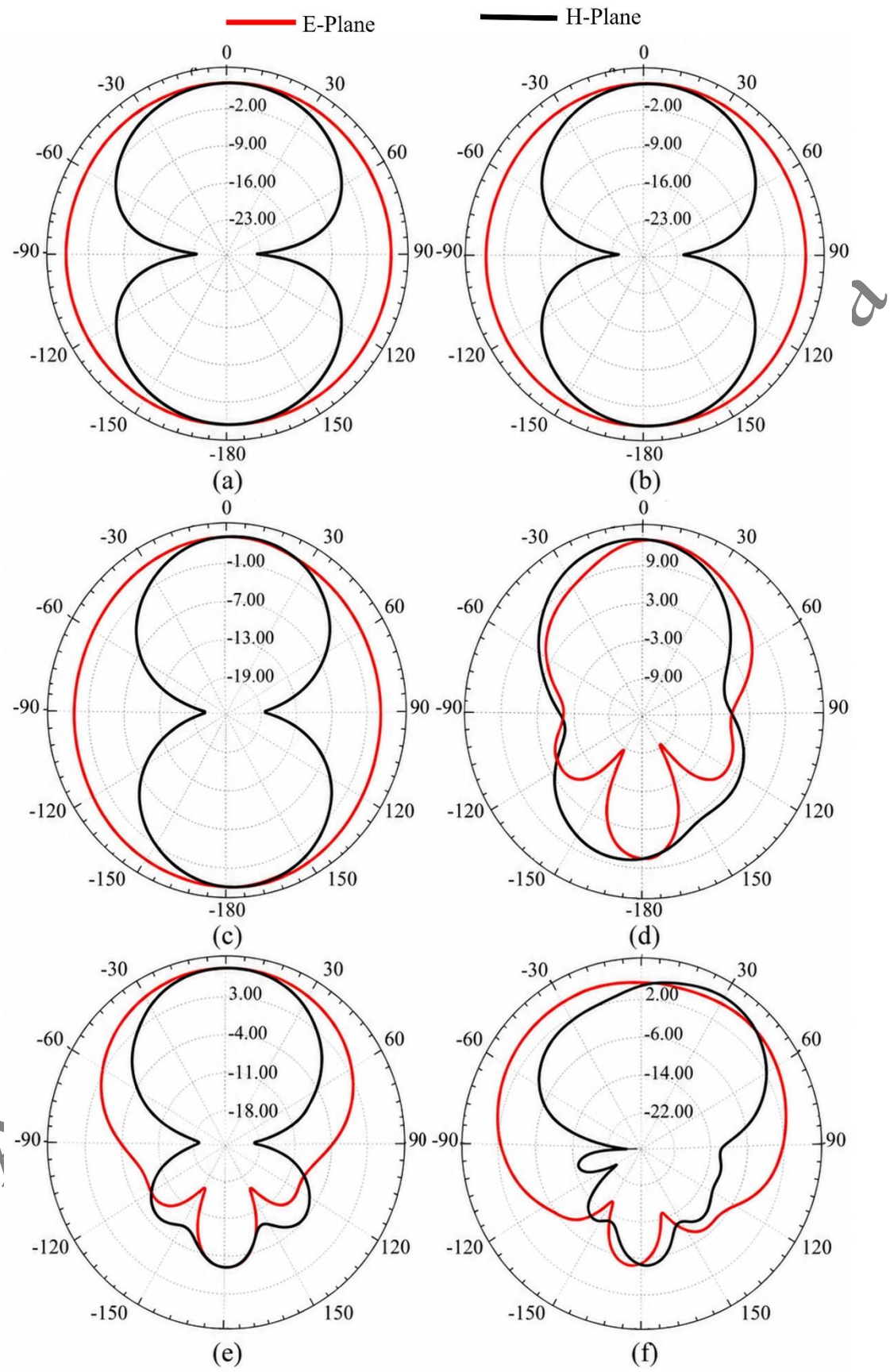

Figure 16 Radiation pattern without FSS at (a) 4 GHz, (b) 5 GHz, (c) 6 GHz, and with FSS at (d) 4 GHz, (e) 5 GHz, (f) 6 GHz

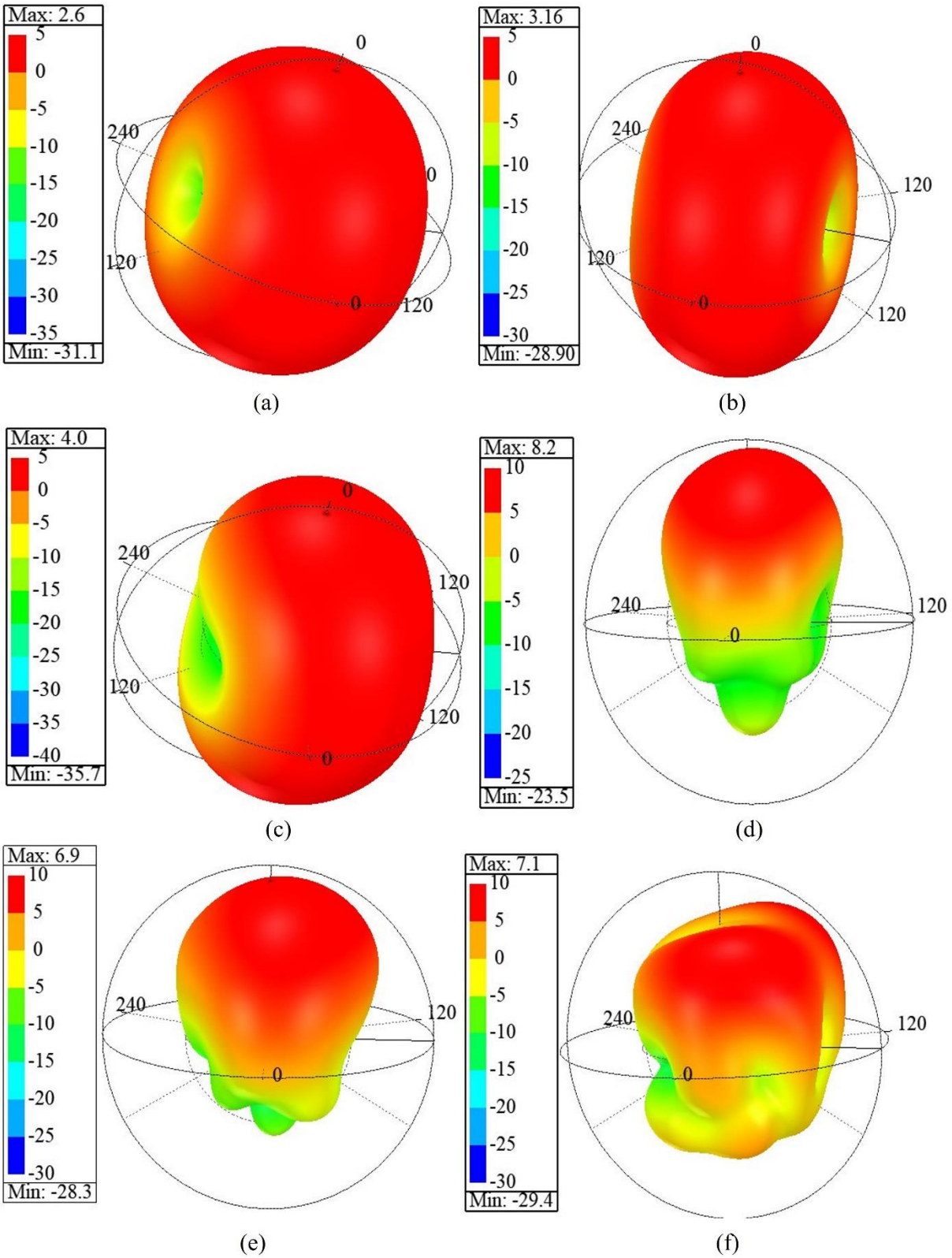

Figure 17. 3D Gain plot of the Proposed Antenna without FSS (a) 4 GHz (b) 5 GHz (c) 6 GHz and with FSS (a) 4 GHz (b) 5 GHz (c) 6 GHz

Table 1. Commonly Operating Frequency Bands Used Worldwide in the Sub-6 GHz Spectrum

Region	Sub-6 GHz Bands		
China	3.3-3.6 GHz	4.5-5 GHz	
UK	3.4-3.8 GHz		
USA	3.45-3.7 GHz, 3.7-3.98GHz	4.49-4.99 GHz	5.9-7.1 GHz
Canada	3.47-3.65 GHz, 3.65-4.0 GHz		5.9-7.1 GHz
Australia	3.4-3.7 GHz		
Italy	3.6-3.8 GHz		
India	3.4-3.6 GHz		
Malaysia	3.5 GHz		
Korea	3.4-3.7GHz, 3.7-4.0 GHz		
Japan	3.6-4.1 GHz	4.5-4.9 GHz	
EU	3.4-3.8 GHz		5.9-6.4 GHz

Table 2: Dimensions of the Proposed Antenna

Parameters	Value (mm)	Parameters	Value (mm)
L_{Sub}	29	L_5	1.4
W_{Sub}	22	W_2	6.1
a	9.5	$W_3=W_1$	5.2
b	10.5	W_4	9
L_f	7	W_5	4
W_f	2.2	W_6	2
L_1	5.1	L_g	7.4
L_2	6.5	t_1	0.7
$L_3=L_4$	1	t	1.2

Table 3. Optimized values of circuit elements of single antenna (R in Ω, C in pF, and L in nH)

Circuit Element	Value	Circuit Element	Value
R1	51	C3	0.62
R2	105	L1	0.92
C1	1.41	L2	0.65
C2	0.77	L3	0.83

Table 4. Design Parameters of the FSS

Parameter	Value (mm)	Parameter	Value (mm)
X	20	R_1	9.8
Y	20	R_2	6
X_1	6.7	S	1.8
X_2	9.25	L_t	80
X_3	2.3	W_t	80

Accepted by Scientia Iranica

Table 5. Optimized Values of Circuit Elements

Circuit Element	Value (Ω)	Circuit Element	Value (nH)	Circuit Element	Value (pF)
R_1	7.5	L_1	0.90	C_1	1.5
R_2	1	L_2	0.80	C_2	1.35
R_3	5	L_3	1	C_3	0.7

Table 6. Comparative Analysis with Reported Antennas in Literature

Ref.	Size of Antenna (mm^2)	Size of FSS (mm^2)	Op. Freq. (GHz)	BW (GHz)	Max. Gain and (Efficiency) without FSS (dBi)	Max. Gain and (Efficiency) with FSS (dBi)
[8]	30×30	98×98	3.6-6.1	2.50	3.8 (>94%)	7.87, (94%)
[9]	18×20	45×30	3.9-5.4	1.50	1.6, (NC)	6 (NC)
[24]	26×31.5	NA	3.28-3.9,5.65-6.25	0.62, 0.60	7, 6, (NC)	NA
[34]	19×43 (2 Port)	117.4×94.9	3-6 GHz	3	3.63, (NC)	7.96 (97%)
[40]	40×40	60×60	8.87-9.20, 10.71-11.54	0.33, 0.83	5.8 (62%)	8.5, 79%
[42]	30×50 (2 Port)	NA	2.9–3.9 5.56–6.25	1, 0.69	4 (70%, 84%)	NA
[43]	59×59	NA	5.12–8.58	3.46	5.58 (NC)	NA
[44]	58×52	162×162	1.52-1.64	0.12	1.65 (68%)	7.3 (76%)
[45]	30×24 and 50×50 (4 Port)	60×60	5.9	0.75558	4, NC	2.7-7.4, (87.45%)
[46]	32×24	80×80	5.92	0.230	3.9 (NC)	5.4 (67.13%)
P. W.	22×29	80×80	3.18-6.35	3.17	4.65 (>87%)	8.62 (>98%)

*P.W.-Proposed Work, NA-Not Applicable, NC-Not Calculated

Accepted by Scientia Iranica

Biography:

Chandra Shekhar Rajora is currently working as an Associate Professor at the Department of Electronics and Communication, School of Engineering and Technology, Jaipur National University, Jaipur, Rajasthan, India. He completed his B.E. in Electronics and Communication Engineering from the University of Rajasthan, Jaipur, and obtained his M.Tech in Digital Communication Engineering from Rajasthan Technical University, Kota, Rajasthan, India. He has more than 19 years of teaching experience at reputable universities. He is a lifetime member of the Indian Society of Technical Education. His special fields of interest are Optical Fiber Communication Systems, Antenna Design and VLSI design.

Prem Pal Singh is currently working as an Assistant Professor in the Department of Electronics and Communication Engineering at Parul University, Vadodara, India. He received his B.Tech. degree in 2015, M.Tech. degree in 2017, and Ph.D. in reconfigurable antenna design from Jaipur National University, Jaipur, India, in 2021. His research interests include wideband and multiband antennas, MIMO antennas for 5G/6G applications, reconfigurable antennas, frequency selective surfaces, and RF circuits. He has published research papers in

reputed journals and conferences and serves as a reviewer for various journals. His current research focuses on compact antennas for wireless communication, mmWave, IoT, and emerging technologies.

Sudhir Kumar Sharma received the Ph.D. degree in Electronics from Delhi University in 2000. He has been associated with teaching and research for the last 25 years in reputed organizations in India and abroad. His research interests include optical communication, IoT, and antenna design. He has authored and co-authored more than 170 national and international publications along with 9 patents. He has guided several research scholars toward their Ph.D. degrees and participated in many national and international conferences worldwide. He received the Senior Research Fellowship from CSIR, New Delhi, in 1997 and the Shiksha Rattan Puruskar in 2013 for academic excellence.

Accepted by Scientia Iranica